Письма в ЭЧАЯ. 2014. Т. 11, № 4(188). С. 637–643

EVENT STRUCTURE INVESTIGATION OF AuAu INTERACTIONS FROM THE HIJING MODEL USING FRACTAL DIMENSIONS

I. Zh. Bunzarov [a,b], *N. Y. Chankova-Bunzarova* [a,b], *O. V. Rogachevsky* [a,c]

[a] Joint Institute for Nuclear Research, Dubna

[b] Institute for Nuclear Research and Nuclear Energy, Sofia

[c] Petersburg Nuclear Physics Institute RAS, Gatchina, Russia

This work presents an implementation of fractal geometry methods in the study of event structure for AuAu interactions at collision energies $\sqrt{s_{NN}} = 9.2, 62$ and 200 GeV for different interaction dynamics. The events are generated by using the HIJING model. It is shown, that the fractal dimensions of events in phase-space projections rapidity–transverse momentum $y-p_t$ and azimuthal angle–transverse momentum $\varphi - p_t$ are sensitive to the interaction dynamics.

Рассматривается приложение метода вычисления фрактальной размерности к исследованию структуры событий AuAu-взаимодействий при энергиях столкновений $\sqrt{s_{NN}} = 9{,}2, 62$ и 200 ГэВ и различной динамике взаимодействий. События были смоделированы генератором HIJING. Показано, что фрактальные размерности событий в проекциях фазового пространства быстрота–поперечный импульс $y - p_t$ и азимутальный угол – поперечный импульс $\varphi - p_t$ чувствительны к динамике взаимодействий.

PACS: 25.75.-q; 25.75.Gz

INTRODUCTION

One of the central goals of experiments in high-energy heavy-ion collisions is the investigation of nuclear matter under extreme conditions of high density and temperature. The most impressive results of high-energy heavy-ion research so far concern the new collective phenomena observed in these reactions — possible formation of Quark Gluon Plasma (QGP) [1].

There are several signatures of QGP, observed in other experiments [2]. One of them is the «jet quenching». Jets are beams of particles produced when pairs of very energetic quarks are knocked out from a proton or neutron during a collision between atomic nuclei. The quarks, going in opposite directions, quickly transform into two jets that fly out in opposite directions from the nuclear fireball. The jets, while moving through the dense medium, will sometimes get slowed down or absorbed. This jet energy absorption is called «jet quenching». By detecting and studying the jet quenching, one should be able to discover the properties of the produced dense medium.

A few known attempts to classify multiple production events according to the fractal dimensions of the distribution of secondary particles in the rapidity space have been initiated

in the work by I. Dremin [3]. Developing the idea, in [4] the box-counting fractal dimension of particle distributions in rapidity, azimuthal angle and transverse momentum variables was used for the analysis of the STAR experimental data. This analysis has revealed that events with different fractal dimensions correspond to different event structures in phase space. Further, in the work [5] it was shown that most of the features observed in relativistic nuclear collisions could be explained as changing of events structure.

The aim of this work is to estimate the sensitivity of the event fractal dimension in both the rapidity–transverse momentum $y - p_t$ and azimuthal angle–transverse momentum $\varphi - p_t$ planes to the interaction dynamics and the use of the fractal dimension for events taxonomy.

1. TYPES OF THE GENERATED HIJING EVENTS

The following three sets of the HIJING events were generated for AuAu interactions investigation: the HIJING default [6] with jet quenching switched on, with jet quenching switched off and without jet production. These types of sets were applied for 9.2, 62 and 200 GeV collision energies. For each set-up and energy 50000 events were generated. Central collisions were chosen because jet quenching effects are most significant in this area and, moreover, the event multiplicity is higher. The analysis was applied to all generated charged particles, under the conditions that the rapidity and transverse momentum were chosen $|y| < 0.7$ and $p_t > 0.15$ GeV/c. The mean event multiplicities are shown in the Table.

Event multiplicities in AuAu interactions at $\sqrt{s_{NN}} = 9.2, 62$ and 200 GeV

Coverage	$\sqrt{s_{NN}}$, GeV	Jet on		Jet off
		Quenching off	Quenching on	
4π	200	9090 ± 366.6	9785 ± 438	4950 ± 117.2
	62	4701 ± 150.1	4687 ± 146.4	3889 ± 106.9
	9.2	1870 ± 38.6	1870 ± 38.72	1870 ± 38.55
$\|y\| < 0.7$, $p_t > 0.15$ GeV/c	200	870.9 ± 59.05	1059 ± 77.43	313.6 ± 20.57
	62	534.3 ± 35.66	526.8 ± 34.57	348.7 ± 22.44
	9.2	350.7 ± 18.67	350.7 ± 18.63	350.8 ± 18.69

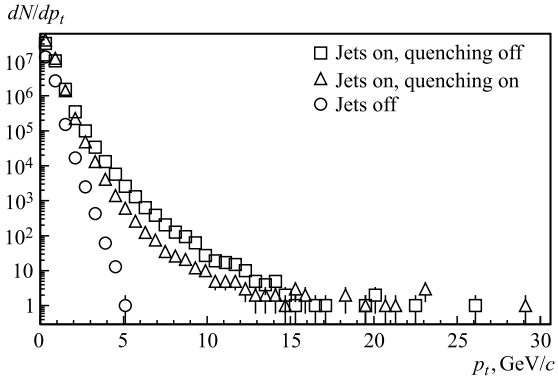

Fig. 1. The p_t distributions of events generated with jet quenching switched on, with jet quenching switched off and without jet production at $\sqrt{s_{NN}} = 200$ GeV

The p_t distributions of events generated with jet quenching switched on, with jet quenching switched off and without jet production at 200 GeV are shown in Fig. 1. It can be seen that the p_t distributions of events generated without jet production have exponential shape and the shape of the p_t distributions of events generated with jet production has a power-law behaviour.

2. FRACTAL DIMENSION CALCULATION

2.1. The Method. For fractal dimension calculation we use one of the most common methods — the box-counting method. The box-counting dimension is a kind of Mandelbrot's fractal dimension [7] usually used for self-similarity objects measuring, but it can be applied, as well, to structures without self-similarity. To explain the method we will use, for example, one of the generated events. These event phase-space projections on the rapidity–transverse momentum $y - p_t$ (plot *a*) and azimuthal angle–transverse momentum $\varphi - p_t$ (plot *b*) planes, are shown in Fig. 2.

If we cover one of these distributions with a grid of n boxes with a length of the edge ε, and after that reduce the edge length ε of the grid, we will obtain a relation between the number of non-empty boxes $n(\varepsilon)$ and the inverse box length ε^{-1}. In a double-logarithmic scale this dependence looks like the one shown in Fig. 3.

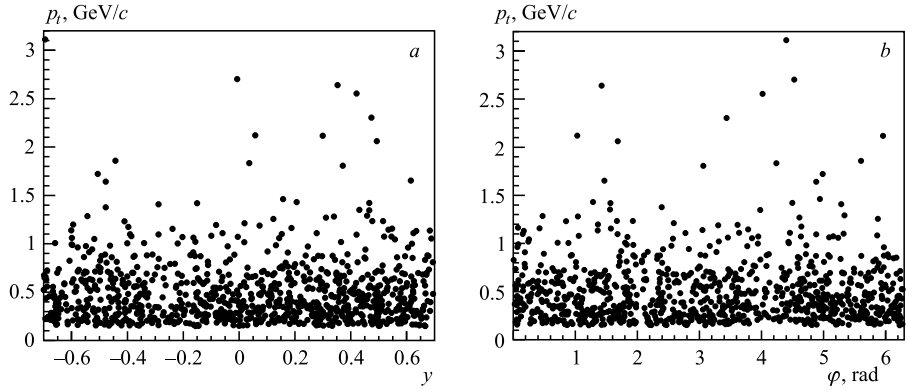

Fig. 2. Phase-space projections on the rapidity–transverse momentum $y - p_t$ (*a*) and azimuthal angle–transverse momentum $\varphi - p_t$ (*b*) planes, with multiplicity of 917 particles

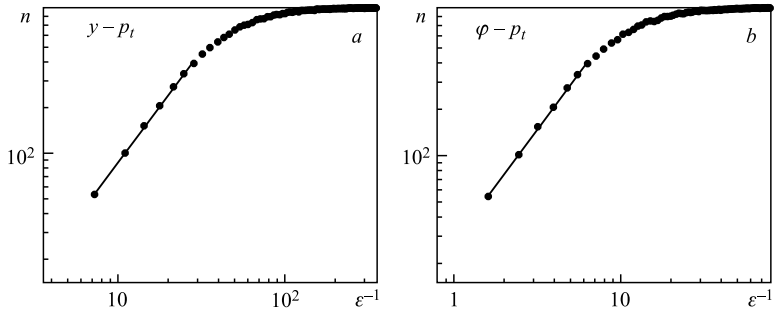

Fig. 3. The $n(\varepsilon^{-1})$ distributions in phase-space projections rapidity–transverse momentum $y - p_t$ (*a*), and azimuthal angle–transverse momentum $\varphi - p_t$ (*b*), in a double-logarithmic scale. The solid lines show the linear fit of the $n(\varepsilon^{-1})$ relation at small ε

In the box-counting method the fractal dimension D is defined by the limit

$$D = \lim_{\varepsilon \to 0} \frac{\log n(\varepsilon)}{\log 1/\varepsilon}.$$

This implies that for small values of ε one asymptotically has

$$D \simeq \frac{\log n(\varepsilon)}{\log 1/\varepsilon} \quad \text{or} \quad n(\varepsilon) \simeq \varepsilon^{-D},$$

i.e., the fractal dimension D can be calculated by evaluating the slope of the linear part of the $n(\varepsilon)$ distribution in a double-logarithmic scale, see Fig. 3. The limited resolution of the data points is reached when ε is small enough so that all the points lie in different boxes, which leads to saturation of the function $n(\varepsilon)$. Obviously, the values of this function near saturation should be disregarded.

The $y - p_t$ and $\varphi - p_t$ distributions are represented as 2D histograms. The boundaries of the histograms are chosen in the following way. For each event we find the largest value of $p_t^{\max}$. For the rapidity axis the boundaries are set from –0.7 to 0.7, and for the azimuthal angle axis — from 0 to 2π rad, for the p_t axis — from 0 to $p_t^{\max}$.

First, the initial number of bins nbin $\times$ nbin is chosen. From the bin size of one of the axes the first value of ε_1 is set and, correspondingly, $n(\varepsilon_1)$. Depending on the chosen step of changing the bins number, the next histogram partition (nbin + step) $\times$ (nbin + step) is determined. Hence, from the bin size in the same axis, ε_2 and the corresponding $n(\varepsilon_2)$ are determined, and so on. Thus, we obtain the distribution of $n(\varepsilon)$. The partitioning of a 2D histogram is performed until the saturation in the distribution of $n(\varepsilon)$ takes place.

The distribution of $n(\varepsilon)$ is put into another 2D histogram. The boundaries of this histogram are determined by the values of $n(\varepsilon^{-1})$ and ε^{-1} in a log–log scale. The next step consists in the selection of the linear part of the distribution. Since the automatic method is still at the stage of development, in the present investigation the linear part is chosen in the following way. In the different events the linear part of $n(\varepsilon^{-1})$ is different and depends on some parameters. So, we determine the longest length to be used for all the other events, from the events with a shortest linear part. That part of the distribution, which is linear in the log–log scale, is fitted by the function $P_0 n(\varepsilon^{-1})^{P_1}$, where P_0 and P_1 are parameters of the fit. The power exponent P_1 gives the slope of the distribution $n(\varepsilon^{-1})$ in the log–log scale which, by definition, is the fractal dimension D of the distributions of $y - p_t$ and $\varphi - p_t$.

2.2. Henon Map Method Test. We test our method for a classical Henon map strange attractor [8], generated with multiplicity of 1000 points, Fig. 4, *a*. The attractors $n(\varepsilon^{-1})$ distribution fit is shown in Fig. 4, *b*. The Henon map is a discrete-time dynamical system that demonstrates chaotic behaviour. In a plane (x, y), the Henon map is given with a set of equations of a kind:

$$x_{n+1} = y_n + 1 - a x_n^2, \quad y_{n+1} = b x_n.$$

For a classical Henon map the values of the parameters are $a = 1.4$ and $b = 0.3$. For the classical map, an initial point of the plane will either approach a set of points known as the Henon strange attractor (which is a fractal), or diverge to infinity.

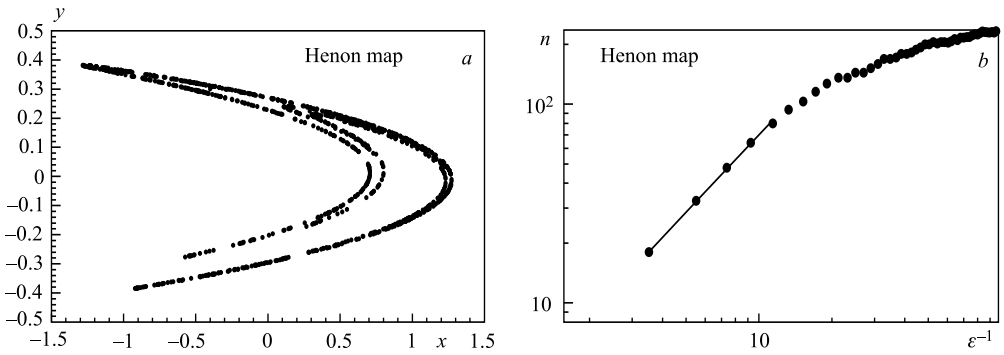

Fig. 4. Classical Henon map strange attractor view (*a*), and the $n(\varepsilon^{-1})$ distribution in a double-logarithmic scale (*b*). The solid line shows the linear fit of the $n(\varepsilon^{-1})$ relation at small ε

In result for the fractal dimension of this distribution our method gives the value of 1.268 ± 0.031, that is very close to the value of 1.261 ± 0.003, calculated in [8].

3. DISCUSSION

As is well known from the other branches of science, the fractal dimension of objects changes under a phase transition [7]. So, it could be expected, that event-by-event analysis using the fractal dimension as a quantitative measure may reveal the existence of possible phase transitions of QGP. With this aim we calculate and study the distributions of the fractal dimensions of particles in the rapidity–transverse momentum $y - p_t$ and azimuthal angle–transverse momentum $\varphi - p_t$ phase-space projections.

The plots in Fig. 5 represent results of fractal dimension calculation in the $y - p_t$ phase-space projection. One can see that at $\sqrt{s_{NN}} = 9.2$ GeV, Fig. 5, *a*, there is no difference in the fractal dimension distributions for events generated with jet quenching, without jet quenching and without jet production.

With energy increment of 62 GeV in events generated with jet production, see Fig. 5, *b*, a shoulder on the right side of the distributions begins to appear. The shoulder in events without jet quenching is approximately twice higher than in events with jet quenching. In the case of energy 200 GeV, Fig. 5, *c*, these shoulders become higher and, once again, for events without jet quenching the shoulder is approximately twice higher than for those with jet quenching. The events without jet production stay without a shoulder.

Quite interestingly, similar results we obtain for the $\varphi - p_t$ phase-space projection. In the plots of Fig. 6, evaluations of the fractal dimension in the $\varphi - p_t$ phase-space projection are shown. As in the $y - p_t$ phase-space projection at $\sqrt{s_{NN}} = 9.2$ GeV, Fig. 6, *a*, there is no difference in the fractal dimension distributions for events generated with jet quenching, without jet quenching and without jet production.

However, for a higher energy 62 GeV, see Fig. 6, *b*, the fractal dimension starts to separate events into two groups for generations with jet production. At $\sqrt{s_{NN}} = 200$ GeV, Fig. 6, *c*, the shoulder becomes more pronounced. The generations without jet production stay still without a shoulder.

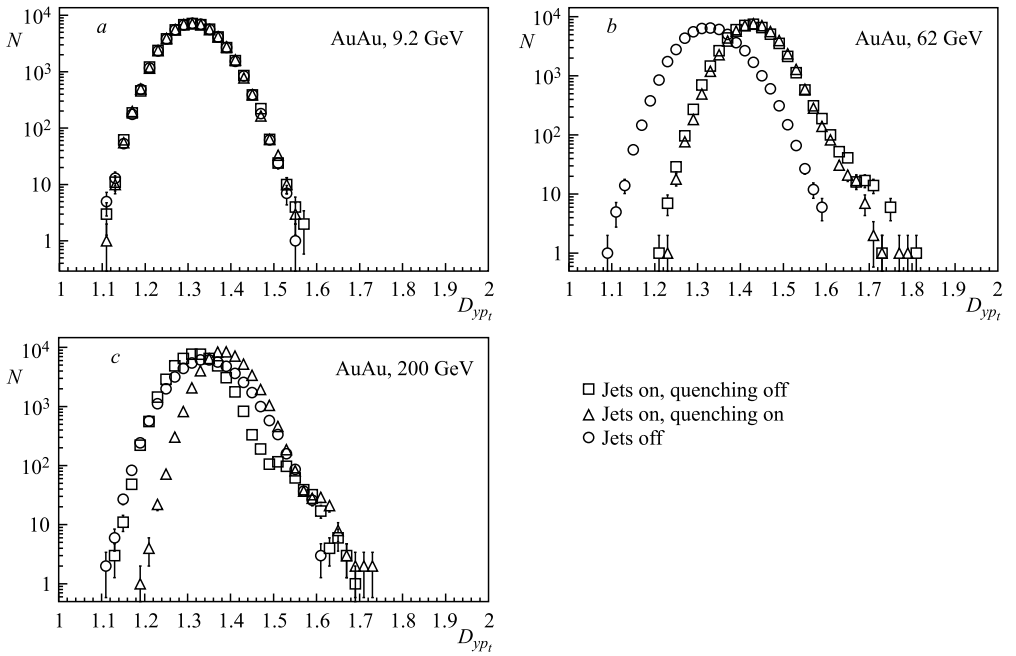

Fig. 5. Fractal dimension distributions of AuAu collisions in $y - p_t$ space at $\sqrt{s_{NN}} = 9.2$ GeV (*a*), 62 GeV (*b*) and 200 GeV (*c*). The curves are shown with the same symbols as in Fig. 1

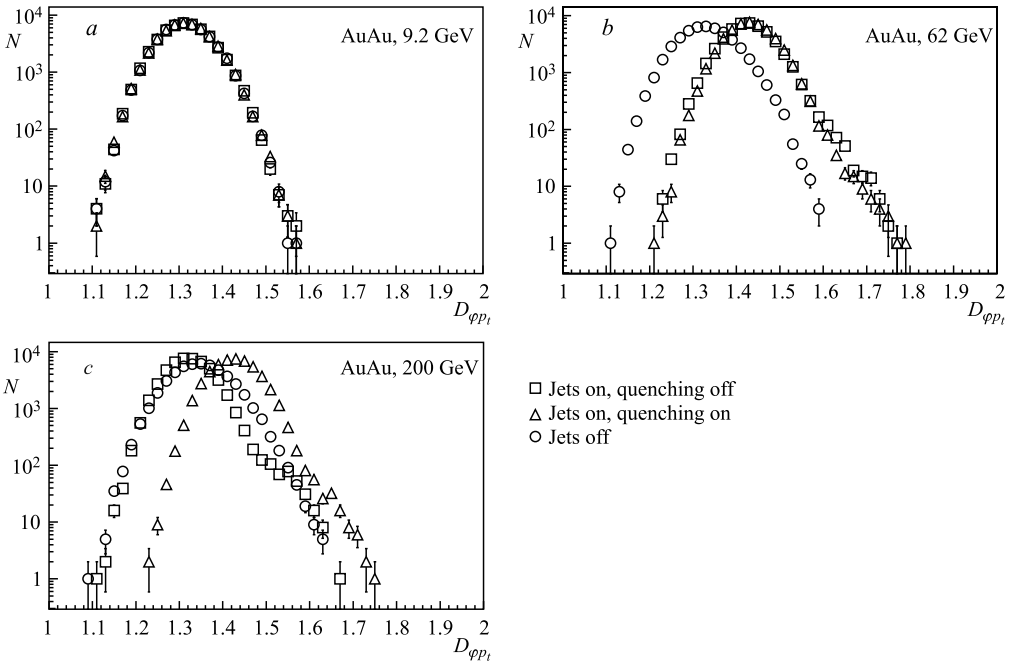

Fig. 6. Fractal dimension distributions of AuAu collisions in $\varphi - p_t$ space at $\sqrt{s_{NN}} = 9.2$ GeV (*a*), 62 GeV (*b*) and 200 GeV (*c*). The curves are shown with the same symbols as in Fig. 1

Thus, the appearance of a shoulder in the distributions of the fractal dimensions in the $y-p_t$ and $\varphi-p_t$ phase-space projections gives a clear evidence for a different interaction dynamics. It is interesting to note that calculations in the $y-\varphi$ phase-space projection do not show such results. One may conjecture that the dependence on the transverse momentum is crucial for the discrimination of events with and without jet production at high interaction energies.

4. SUMMARY

The fractal dimension calculation analysis of multiparticle events in the $y-p_t$ and $\varphi-p_t$ phase-space projections shows, that with the raising of the interaction energy, the events start to divide into two kinds, i.e., the method distinctly separates two classes of events with different fractal dimension, that is with different particle-production dynamics in these interactions. This perspective has motivated the choice of the energy values used in the present analysis of the generated HIJING events. However, our analysis has been confined to events generated by central collisions, while the real data will introduce the effect of noncentral collisions as well.

Acknowledgements. The authors are grateful to M. V. Tokarev for useful comments and remarks.

REFERENCES

1. The Quark Matter 2012: Proc. of the XXIII Intern. Conf. on Ultrarelativistic Nucleus–Nucleus Collisions, Washington D. C., USA, Aug. 13–18, 2012 / Ed. by Th. Ullrich, B. Wysouch and J. W. Harris // Nucl. Phys. A. 2013. V. 904–905. P. 1c–1092c.
2. *Adams J. et al.* Experimental and Theoretical Challenges in the Search for the Quark–Gluon Plasma: The STAR Collaboration's Critical Assessment of the Evidence from RHIC Collisions // Nucl. Phys. A. 2005. V. 757. P. 102–183.
3. *Dremin I.* The Fractal Correlation Measure for Multiple Production // Mod. Phys. Lett. A. 1988. V. 3, No. 14. P. 1333–1335.
4. *Rogachevsky O. V.* Scale-Dependent Analysis Approach for STAR Events // Proc. of the 33rd Intern. Conf. on High-Energy Physics. 2006. V. 1. P. 443–445.
5. *Rogachevsky O.* Study of the Multiparticle Events Structure with Fractal Geometry Methods // Nucl. Phys. B (Proc. Suppl.). 2011. V. 219–220. P. 305–307.
6. *Wang X-N., Gyulassy M.* HIJING: A Monte Carlo Model for Multiple Jet Production pp, pA, and AA Collisions // Phys. Rev. D. 1991. V. 44. P. 3501.
7. *Feder J.* Fractals. N. Y.: Plenum Press, 1988.
8. *Russel D. A., Hanson J. D., Ott E.* Dimension of Strange Attractors // Phys. Rev. Lett. 1980. V. 45, No. 14. P. 1175.

Received on November 14, 2013.